STRESS AND SHAPE ANALYSIS OF A PARAGLIDER WING

By Robert W. Fralich

NASA Langley Research Center
Langley Station, Hampton, Va.

Presented at the Winter Annual Meeting of ASME

New York, New York
Nov. 29 - Dec. 4, 1964

STRESS AND SHAPE ANALYSIS OF A PARAGLIDER WING[1]

By Robert W. Fralich[2]

SUMMARY

29∠82

A combined aerodynamic-structural analysis is made which is based on the assumption that the sail is flexible and has freedom to take the shape which the aerodynamic pressure and the internal stresses dictate. Numerical results were obtained for Newtonian impact aerodynamic theory and were compared with published results obtained for a rigid idealization of the paraglider wing. It was found that the assumed rigid idealization did not approximate the shape of a flexible wing well and led to significant errors in the lift and drag forces and the lift-to-drag ratio. The new calculations provide a basis for design of para- gliders for hypersonic flight.

author

INTRODUCTION

The paraglider wing is under active development as a controllable lifting device for landing space vehicles. It has also been suggested for other applications such as recovering rocket boosters and effecting reentry into the earth's atmosphere. A typical configuration is shown in figure 1. $\left(\text{See also } [1]^3.\right)$ It consists of leading-edge booms and a keel boom joined together at the nose

---

[1]This paper is based on a dissertation submitted in partial fulfillment of the requirements of the degree of Doctor of Philosophy at Virginia Polytechnic Institute, Blacksburg, Virginia, June 1963.

[2]Aerospace Engineer, NASA Langley Research Center, Langley Station, Hampton, Virginia.

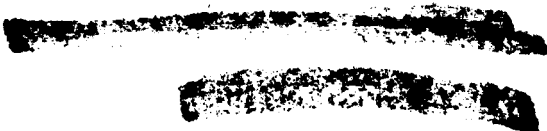[3]Numbers in brackets designate references at end of paper.

L-4098

and a flexible sail whose surface carries the aerodynamic pressure loading. The payload is usually suspended beneath the wing by shroud lines. The distance between booms is often constrained by use of spreader bars or by means of a spring mechanism at the nose. Control is afforded by adjusting the length of the shroud lines and thus positioning the payload with respect to the wing.

Various wind-tunnel and free-flight investigations have been made using either flexible or rigid idealizations of paraglider wings in order to find lift and drag characteristics or stability and control characteristics. (See, for example, [1-8].) None of the investigations on flexible sails yielded the deflected shape, the pressure distribution on the sail, or the stresses in the sail. Two investigations [5,6] on rigid idealizations did yield pressure distributions. However, these distributions apply to the fixed shape of the idealized wing and only represent the distribution on an actual flexible sail if the rigid idealization corresponds to the actual deflected shape of the flexible wing.

In this paper a theoretical investigation is made which consists of a combined structural and aerodynamic analysis. In this analysis, the sail is assumed to be an inextensional, flexible membrane which has complete freedom to take the shape which the aerodynamic pressures and the internal stresses dictate. The assumptions are also made that the booms are rigid and straight and that they have small enough cross sections so as not to affect the aerodynamics. The booms are maintained a fixed distance apart by spreader bars, and the dihedral of the leading-edge booms is fixed with respect to the keel boom.

The aerodynamic theory used is Newtonian impact theory, which has sometimes been used to express the aerodynamic pressure-shape relationship for the hypersonic speed range. (See, for example, [9,10].) This choice of aerodynamic

theory is governed by two factors. First, Newtonian theory leads to a simplified analysis which shows the applicability of the present approach in a simple manner. Second, this aerodynamic theory has been applied in [7] to a rigid idealization of a paraglider wing, and thus serves as a basis of comparison for the numerical results. Numerical results are obtained for a flexible configuration that corresponds to this rigid idealization in the sense that it has the same surface planform and the same keel and leading-edge locations. The variations of lift and drag coefficients with angle of attack are compared with those for the rigid idealization and the deflected shape, pressure distribution, and stress resultants in the sail are determined. Also, numerical results are presented to show effects of variation in dihedral angle (raising or lowering of the leading-edge booms).

GOVERNING EQUATIONS

Geometry of the Sail

In this analysis the sail is assumed to be constructed from a flat, inextensional membrane which may take some rather general shape in its loaded equilibrium condition. By virtue of its inextensibility, it is possible to establish appropriate coordinates in the surface by considering the sail in its flat (unloaded) condition. (See fig. 2(a).) Points on the sail are thus designated by the coordinates x and θ. Since the paraglider wing is symmetric about the x_1 axis (fig. 1), and since only symmetric deformations and loadings will be considered herein, only that portion of the wing in the first quadrant need be considered. The keel boom, of length l_K, is located at $\theta = 0$ and the leading-edge boom, of length l_L, at $\theta = \theta_L$. It is also assumed that the trailing edge of the sail is straight; points on the trailing edge are

expressed by the equation

$$x_T = \frac{\mathit{l}_K A}{\sin \theta + A \cos \theta} \qquad (1)$$

where

$$A = \frac{\sin \theta_L}{\dfrac{\mathit{l}_K}{\mathit{l}_L} - \cos \theta_L} \qquad (2)$$

and a subscript T has been added to indicate that the values of x from this equation are values at the trailing edge.

For the x, θ polar coordinate system, the first fundamental form is given by

$$ds^2 = dx^2 + x^2 \, d\theta^2 \qquad (3)$$

Since the booms are straight and rigid and lie on x-coordinate lines and since deformations of the sail are assumed inextensional, the x, θ coordinate curves are lines of principal curvature of the loaded surface for which

$$\left. \begin{array}{l} R_1 = \infty \\[2ex] R_2 = \dfrac{x^2}{g} \end{array} \right\} \qquad (4)$$

are the radii of principal curvature. This is a surface of zero Gaussian curvature which has the second fundamental form $g d\theta^2$. Note that the sign convention on g differs from that usually employed in references in differential geometry of surfaces in that, for positive curvature of the surface, the positive direction of the normal is outward. The only one of the Codazzi equations of compatibility $\left(\text{see } [11] \right)$ not identically satisfied becomes

$$\frac{\partial g}{\partial x} = \frac{g}{x} \tag{5}$$

Integration of equation (5) yields

$$g = \frac{x}{R(\theta)} \tag{6}$$

where $R(\theta)$ is an arbitrary function of θ alone. Then the radius of curvature R_2 (eq. (4)) is

$$R_2 = xR(\theta) \tag{7}$$

Equilibrium Equations

Equilibrium of the loaded sail is governed by the equilibrium equations of membrane shells of zero Gaussian curvature $\left(\text{see, for example, } [12]\right)$. In terms of the x,θ coordinates, these are:

$$xN_{x,x} + N_{x\theta,\theta} + N_x - N_\theta = 0 \tag{8}$$

$$xN_{x\theta,x} + N_{\theta,\theta} + 2N_{x\theta} = 0 \tag{9}$$

$$N_\theta = R_2 X = x(RX) \tag{10}$$

for the case where only normal pressure forces X act on the surface of the sail. Here N_x and N_θ are the normal stress resultants in the x and θ directions, respectively, and $N_{x\theta}$ is the shearing stress resultant. The comma followed by a subscript denotes partial differentiation with respect to this subscript.

Boundary Conditions

It is appropriate to consider force boundary conditions along a general boundary contour C of the loaded surface. Thus, one may prescribe

$$\left.\begin{array}{l} P_L = l_1^2 N_x + 2l_1 l_2 N_{x\theta} + l_2^2 N_\theta \\[2ex] P_S = l_1 s_1 N_x + \left(l_1 s_2 + l_2 s_1\right) N_{x\theta} + l_2 s_2 N_\theta \end{array}\right\} \tag{11}$$

where P_L and P_S are applied boundary forces per unit length in the surface normal and tangent to C, respectively. Here l_1 and l_2 are the components of the unit outward surface normal $\overline{L}$ to C and s_1 and s_2 are the components of the unit tangent $\overline{S}$ (in the direction of increasing $\overline{S}$). Since $\overline{L}$ and $\overline{S}$ are orthogonal vectors

$$s_1 l_1 + s_2 l_2 = 0 \tag{12}$$

$$s_1^2 + s_2^2 = 1 \tag{13}$$

$$l_1^2 + l_2^2 = 1 \tag{14}$$

From figure 3 it can be seen that

$$\left.\begin{array}{l} s_1 = \dfrac{dx}{ds} \\[3ex] s_2 = x\,\dfrac{d\theta}{ds} \end{array}\right\} \tag{15}$$

For a given boundary contour C, s_1 and s_2 can be found from equations (13) and (15) and l_1 and l_2 from equations (12) and (14). Then the force boundary conditions for the given contour are determined from equations (11).

Trailing-edge boundary conditions.- At the trailing edge the boundary contour is expressed by equation (1). From equations (1) and (15) the following is obtained:

$$(\sin \theta + A \cos \theta)s_1 + (\cos \theta - A \sin \theta)s_2 = 0 \qquad (16)$$

Simultaneous solution of equations (13) and (16) together with the solution of equations (12) and (14) yields

$$s_1 = -l_2 = -\frac{1}{\sqrt{1 + A^2}}(\cos \theta - A \sin \theta) \qquad (17)$$

$$s_2 = l_1 = \frac{1}{\sqrt{1 + A^2}}(\sin \theta + A \cos \theta) \qquad (18)$$

Now application of equation (11) along a stress-free trailing edge yields

$$\left(P_L\right)_T = \frac{1}{1 + A^2}\left[(\sin \theta + A \cos \theta)^2\left(N_x\right)_T \right.$$
$$+ 2(\cos \theta - A \sin \theta)(\sin \theta + A \cos \theta)\left(N_{x\theta}\right)_T$$
$$\left. + (\cos \theta - A \sin \theta)^2\left(N_\theta\right)_T\right] = 0 \qquad (19)$$

and

$$\left(P_S\right)_T = \frac{1}{1 + A^2}\left\{(\sin \theta + A \cos \theta)(\cos \theta - A \sin \theta)\left[\left(N_\theta\right)_T - \left(N_x\right)_T\right]\right.$$
$$\left. + \left[(\sin \theta + A \cos \theta)^2 - (\cos \theta - A \sin \theta)^2\right]\left(N_{x\theta}\right)_T\right\} = 0 \qquad (20)$$

Finally, equations (19) and (20) may be recast in convenient form by solving for $\left(N_{x\theta}\right)_T$ and $\left(N_x\right)_T$ and using equations (1) and (10)

$$\left(N_{x\theta}\right)_T = \left(\frac{dx_T}{d\theta}\right)(RX)_T \tag{21}$$

and

$$\left(N_x\right)_T = \frac{1}{x_T}\left(\frac{dx_T}{d\theta}\right)^2 (RX)_T \tag{22}$$

Nose boundary conditions.- The boundary conditions at the nose of the sail are obtained by considering the limiting case of a stress-free boundary that shrinks to a point. Hence the stress resultants N_x, N_θ, and $N_{x\theta}$ must remain finite at this point.

Keel and leading-edge boundary conditions.- The boundary conditions at the keel and leading edge are given by specifying the relative positions of the keel and leading edge. Details of the specification of these boundary conditions are reserved to a subsequent section.

ANALYSIS

Solution of Equilibrium Equations

Substitution of the expression for N_θ from equation (10) into equations (8) and (9) yields

$$\left(xN_x\right)_{,x} + N_{x\theta,\theta} = x(RX) \tag{23}$$

$$\left(x^2 N_{x\theta}\right)_{,x} = -x^2(RX)_{,\theta} \tag{24}$$

Integration of equation (24) gives

$$N_{x\theta} = -\frac{1}{x^2}\int_0^x \xi^2 (RX)_{,\theta}d\xi \tag{25}$$

where the boundary condition for finiteness of the stress resultant at the nose of the sail has been satisfied. Substitution of $N_{x\theta}$ from equation (25) into equation (23) and integration then yields

$$N_x = \frac{1}{x} \int_0^x \left[\xi(RX) + \frac{1}{\xi^2} \int_0^\xi \lambda^2(RX)_{,\theta\theta}d\lambda \right]d\xi \qquad (26)$$

where again, the boundary condition at $x = 0$ has been imposed. Thus, the stress resultants N_θ, $N_{x\theta}$, and N_x are readily expressed in terms of the aerodynamic pressure $X(x,\theta)$ and the single parameter $R(\theta)$.

Now the boundary conditions (21) and (22) for stress resultants at the trailing edge of the sail are seen to require:

$$-\frac{1}{x_T^2} \int_0^{x_T} \xi^2(RX)_{,\theta}d\xi = \left(\frac{dx_T}{d\theta}\right)(RX)_T \qquad (27)$$

$$\frac{1}{x_T} \int_0^{x_T} \left[\xi(RX) + \frac{1}{\xi^2} \int_0^\xi \lambda^2(RX)_{,\theta\theta}d\lambda \right]d\xi = \frac{1}{x_T}\left(\frac{dx_T}{d\theta}\right)^2(RX)_T \qquad (28)$$

t should be noted that both equations (27) and (28) must be satisfied; how-ver, only the one aribtrary function $R(\theta)$ is available for satisfying these wo conditions. Difficulties of this nature are commonly found when dealing with embrane shells of zero Gaussian curvature $\left(\text{see, for example, } [12]\right)$ and as a result membrane stress states can, in general, be obtained only in special cases. For the straight trailing-edge boundary conditions considered in this problem the fortunate situation arises that, for any aerodynamic pressures of the type

$$X(x,\theta) = \sum_{n=-1}^{\infty} a_n x^n Z_n(\theta) \qquad (29)$$

a single function $R(\theta)$ can be found which satisfies both equations (27) and (28) and thus leads to true membrane stress states. Moreover, for aerodynamic pressures of this type, a straight trailing edge is necessary for obtaining a membrane stress state that satisfies both trailing-edge boundary conditions.

The parameter $R(\theta)$ expresses the shape of the loaded surface of the sail and the aerodynamic pressure $X(x,\theta)$ is dependent on this shape. It is convenient for deriving a relationship between aerodynamic loading and the shape to express the shape in terms of angles $\beta(\theta)$ and $\delta(\theta)$ measured from the keel location rather than by $R(\theta)$. (See fig. 2(b).) In appendix A the parameter $R(\theta)$ is found in terms of β, and δ is related to β via the condition of inextensibility. The resulting equations are:

$$R(\theta) = \frac{-\sqrt{1 - \left(\frac{d\beta}{d\theta}\right)^2}}{\dfrac{d^2\beta}{d\theta^2} + \dfrac{\sin \beta}{\cos \beta}\left[1 - \left(\frac{d\beta}{d\theta}\right)^2\right]} \tag{30}$$

and

$$\frac{d\delta}{d\theta} = \pm \frac{1}{\cos \beta}\sqrt{1 - \left(\frac{d\beta}{d\theta}\right)^2} \tag{31}$$

Application of Newtonian Impact Theory

The entire analysis up to this point is based upon equilibrium consideration of the sail subjected to normal pressure, and the equations derived are not dependent upon any specific aerodynamic theory. In this section use is made of Newtonian impact theory. $\left(\text{See, for example, } [9,10].\right)$ This theory, often used for hypersonic velocities, has the advantage of yielding pressures X

which are functions of θ alone and thus permitting satisfaction of the boundary conditions (27) and (28). In addition, this aerodynamic theory has also been applied in [7] to a rigid idealization of a paraglider wing; therefore, a direct comparison can be made with the results of [7] to evaluate the use of rigid models in the study of paraglider behavior.

In Newtonian impact theory, the pressure at a point is given by the relation

or

$$X = 2q \sin^2\epsilon \quad \text{if} \quad \epsilon \gtreqless 0$$

$$X = 0 \quad \text{if} \quad \epsilon < 0$$

$$(32)$$

where q is the dynamic pressure and ϵ is the angle between the local stream-wise unit tangent vector and the free-stream velocity vector. Newtonian impact theory requires that the moving stream gives up its "normal" component of momentum (to the surface impacted) but retains the tangential component which passes off tangentially to the local surface. Only portions of the surface that "see" the flow have a nonzero pressure coefficient, as indicated in equations (32). The unit normal $\bar{\nu}$ to the surface has been determined in terms of the parameters β and δ in appendix A (see eq. (52)). If it is noted that $\sin \epsilon = \cos(\bar{i}, \bar{\nu}) = \bar{i} \cdot \bar{\nu}$, and use is made of equation (52), the pressure on the sail at a given point (eq. (32)) is readily expressed as

$$X = 2q \left[(\cos \beta \sin \alpha - \sin \beta \cos \delta \cos \alpha) \sqrt{1 - \left(\frac{d\beta}{d\theta}\right)^2} + \sin \delta \cos \alpha \frac{d\beta}{d\theta} \right]^2$$

$$(33)$$

From equation (33), it is evident that X is a function of θ alone. For this case, the boundary conditions (27) and (28) on the stress resultants

12

at the trailing edge of the sail are satisfied by

$$(RX) = \frac{C}{x_T^3} \qquad (34)$$

Here the constant of integration C is to be determined by the relative positions of the keel and leading edge.

Equation (34) upon substitution from equation (33) for X and equation (30) for R yields a differential equation from which the deflected shape of the sail is determined; thus

$$-\sqrt{1 - \left(\frac{d\beta}{d\theta}\right)^2}\left[(\cos \beta \sin \alpha - \sin \beta \cos \delta \cos \alpha)\sqrt{1 - \left(\frac{d\beta}{d\theta}\right)^2} + \cos \alpha \sin \delta \frac{d\beta}{d\theta}\right]^2$$

$$= \frac{1}{2}\left(\frac{C}{q l_K^3}\right)\left(\frac{1}{A}\sin \theta + \cos \theta\right)^3\left\{\frac{d^2\beta}{d\theta^2} + \frac{\sin \beta}{\cos \beta}\left[1 - \left(\frac{d\beta}{d\theta}\right)^2\right]\right\} \qquad (35)$$

One other relation is needed. This is provided by integration of equation (31):

$$\delta = \int_0^\theta \frac{1}{\cos \beta}\sqrt{1 - \left(\frac{d\beta}{d\theta}\right)^2}\,d\theta \qquad (36)$$

The negative sign in equation (31) is ruled out since the lower (or upstream) surface must "see" the flow. Solution of the simultaneous nonlinear equations (35) and (36), for β and δ, and satisfaction of specified conditions $\beta(\theta_L)$ and $\delta(\theta_L)$, at the leading edge of the sail, determines the deflected shape of the sail. This solution is effected by using finite differences to represent derivatives of β with respect to θ:

$$\left.\begin{array}{l} \left(\dfrac{d\beta}{d\theta}\right)_n = \dfrac{1}{2\Delta}\left(\beta_{n+1} - \beta_{n-1}\right) \\[4mm] \left(\dfrac{d^2\beta}{d\theta^2}\right)_n = \dfrac{1}{\Delta^2}\left(\beta_{n+1} - 2\beta_n + \beta_{n-1}\right) \end{array}\right\} \qquad (37)$$

where Δ is the spacing of the stations and station $n = 0$ is taken at the keel. Parabolic integration is employed to evaluate the integral in equation (36) so that

$$\delta_n = \delta_{n-1} + \frac{\Delta}{12}\left(5f_n + 8f_{n-1} - f_{n-2}\right) \tag{38}$$

where

$$f_n = \frac{1}{\cos \beta_n}\sqrt{1 - \left(\frac{d\beta}{d\theta}\right)_n^2}$$

Then, if values of $(d\beta/d\theta)_0$, $\left(c/q l_K^3\right)$, and angle of attack α are specified, equations (35) and (36) became two simultaneous equations for determining δ_n and β_{n+1} in terms of their values at preceding stations. For each set of selected values of $(d\beta/d\theta)_0$, $\left(c/q l_K^3\right)$, and α, these equations are applied successively to obtain a set of values of $\beta(\theta_L)$ and $\delta(\theta_L)$ at the leading edge. The values of $(d\beta/d\theta)_0$ and $\left(c/q l_K^3\right)$ are then varied until the deflected shape with the desired boundary values of $\beta(\theta_L)$ and $\delta(\theta_L)$ is obtained.

The stress resultants may now be evaluated. With the relations (34) for RX, and (1) for x_T equations (10), (25), and (26) become

$$\left.\begin{aligned}
N_\theta &= \left(\frac{c}{q l_K^3}\right)\frac{xq}{A^3}(\sin \theta + A \cos \theta)^3 \\[2ex]
N_x &= \left(\frac{c}{q l_K^3}\right)\frac{xq}{A^3}(\sin \theta + A \cos \theta)(\cos \theta - A \sin \theta)^2 \\[2ex]
N_{x\theta} &= -\left(\frac{c}{q l_K^3}\right)\frac{xq}{A^3}(\sin \theta + A \cos \theta)^2(\cos \theta - A \sin \theta)
\end{aligned}\right\} \tag{39}$$

where A is given by equation (2) and where $\left(\dfrac{C}{q l_K^3}\right)$ has been determined in the course of the numerical integration described above.

Determination of the two principal stress resultants yields the value zero and

$$N = \frac{C}{q l_K^3} \frac{xq}{A^3}\left(1 + A^2\right)(\sin \theta + A \cos \theta) \tag{40}$$

acting perpendicular and parallel to the trailing edge, respectively. From figure 2(a) and equation (1) it can be seen that lines parallel to the trailing edge are given by

$$x = \frac{(x)_{\theta=0} A}{\sin \theta + A \cos \theta} \tag{41}$$

so that along these lines the maximum principal stress resultant is a constant:

$$N = \frac{C}{q l_K^3} \frac{(x)_{\theta=0} q}{A^2}\left(1 + A^2\right) \tag{42}$$

Integration of the stress resultants given by equations (39) at the keel and leading edge yields the resultant forces applied by the sail to the booms. (See fig. 4.) Then by considering the components of the boom forces in the z_0 and x_0 directions, the lift and drag forces are obtained. The boom forces and the lift and drag forces are determined in appendix B.

NUMERICAL RESULTS AND DISCUSSION

Numerical results are presented and discussed for a configuration that corresponds in all possible respects to a rigid idealization analyzed in [7]. This configuration has keel and leading-edge booms of equal length;

and, in the undeflected flat condition, the angle θ_L (between the keel and leading-edge booms) is $45°$. Boundary conditions which locate the leading-edge boom relative to the keel boom are chosen to correspond to the rigid idealization identified in [7] as having "180° canopy inflation." These boundary conditions are given by

$$\beta\left(\theta_L\right) = 0$$

$$\delta\left(\theta_L\right) = 28.2°$$

which yields a distance between the ends of the leading-edge and keel booms equal to

$$d = l_K \sqrt{2 - 2 \cos \beta\left(\theta_L\right)\cos \delta\left(\theta_L\right)}$$
$$= 0.4872 l_K$$

The differential equation (35), for the deflected shape, and its auxiliary equation (36) were solved with finite differences applied at intervals of $\Delta = 1°$ in the variable θ. The problem was programed on a high-speed digital computer, and deflected shapes were calculated for various angles of attack. From the calculated deflected shapes, the pressure coefficient, the stress resultants, the resultant forces applied by the sail to the booms, the lift and drag coefficients, and the ratio of lift to drag were calculated for each angle of attack. These results are given in table 1 and figures 5 through 7. The deflected shape of the surface of the sail is shown by the solid curves in figure 5 for angles of attack of $30°$, $60°$, and $90°$. Comparison with the rigid idealization of [7] (the dashed curve) shows that the rigid idealization is substantially in error at all angles of attack. The variation of pressure

coefficient $C_p = X/q$ with angle of attack is shown in figure 6. Figures 5 and 6 show that, as the angle of attack increases, the point of maximum deflection and the point of maximum pressure coefficient move outboard from the keel.

At any point on the sail, the directions of the principal stress resultants are perpendicular and parallel to the trailing edge. The first one has the value zero for all points on the sail. The other has a constant value N for all points on a line parallel to the trailing edge. This value is obtained by use of equation (42)

$$N = 1.172\left(\frac{C}{q l_K^3}\right)(x)_{\theta=0} q$$

where $(x)_{\theta=0}$ gives the intersection of the line with the keel. The magnitude varies with angle of attack through the constant $\dfrac{C}{q l_K^3}$ which can be obtained by use of table 1. The magnitude N is also proportional to the distance $(x)_{\theta=0}$ from the nose. Note that the maximum stress is at the trailing edge and is a quantity of principal interest in the design of the sail.

The lift and drag characteristics of the flexible wing are compared with those for the rigid idealization in figures 7(a) and 7(b) which show that the arbitrary shape used for the rigid idealization causes an overestimation of the lift and drag forces over the complete range of angle of attack; however, the same trends are apparent for both the rigid and flexible wings. The lift-to-drag ratio (fig. 7(c)) which is a measure of the angle of glide, shows a very significant difference for angles of attack below 50°. Computations were not carried below 25° because of the large amount of computer time needed in order to obtain the deflected shape in this range of angle of attack. This difficulty arises because at low angles of attack small changes in the assumed values of

$c/q l_K^3$ and $(d\beta/d\theta)_0$ produce large changes in the deflected shape. Presumably, L/D drops abruptly at some lower value of α. But the results already show that L/D for the flexible sail is more than three times the maximum value of L/D for the rigid idealization.

The resultant forces, applied by the sail to the keel and leading-edge booms, and the location of these forces are given in table 1. These values may be used by the designer for calculating stresses in shroud lines and spreader bars. Stresses in the booms may then be found by analyzing these booms as free-free beams subjected to the self-equilibrating system of loads provided by the sail, shroud lines, and spreader bars.

Effects of changing the dihedral of the wing were also considered. The boundary conditions for this case correspond to maintaining the value

$$d = 0.4872 l_K$$

and specifying various values of $\beta(\theta_L)$. These computations were performed for an angle of attack $\alpha = 35^\circ$ in order to find deflected shapes, pressure distributions, boom forces, and lift and drag coefficients. The variation of the force characteristics with dihedral is given in table 2. The variation of lift and drag coefficients with dihedral is shown in figure 8. The maximum values of lift and drag coefficients are obtained for a dihedral angle of about -8°.

CONCLUDING REMARKS

Equilibrium equations for the sail of the paraglider wing have been derived and integrated. Results are first obtained in rather general form for the stress resultants in the sail, boom forces and lift and drag in terms of the

pressure on the sail and a parameter that describes the deflected shape of the sail. The specification of an appropriate aerodynamic theory - in the present case, Newtonian impact theory - then permits satisfaction of the boundary conditions at the trailing edge and calculation of the deflected shape of the sail. Finally, the general formulas are applied to calculate the stress resultants, lift, and drag.

Numerical results have been obtained and have been compared with published results for a rigid idealization of the paraglider wing. The comparison shows that the assumed shape of the rigid wing is considerably in error over the complete range of angles of attack. Consequently, the lift and drag coefficients and, especially the lift-to-drag ratio, for the flexible wing are significantly different from the values found for the rigid wing. Thus use of rigid idealizations in wind-tunnel investigations to draw conclusions as to the aerodynamic characteristics of the paraglider - especially the lift-to-drag ratio - may be greatly misleading.

The calculated stress resultants and boom forces provide a basis for design of sails, booms, shroud lines, and spreader bars for a paraglider in hypersonic flight.

APPENDIX A

SHAPE OF LOADED SURFACE OF THE SAIL

In this appendix the shape of the loaded surface of the sail is represented by the angles β and δ shown in figure 2(b)). The x_1-axis of the rectangular Cartesian coordinates x_1, y_1, z_1 is alined with the keel of the paraglider and the $x_1 z_1$-plane is the vertical plane of symmetry of the paraglider. Hence

$$\left. \begin{array}{l} z_1 = x \sin \beta \\[2ex] x_1 = x \cos \beta \cos \delta \\[2ex] y_1 = x \cos \beta \sin \delta \end{array} \right\} \qquad (43)$$

Consider the keel at an angle of attack α and define rectangular Cartesian coordinates x_0, y_0, z_0 such that the x_0-axis is alined with the direction of airflow. The $x_0 z_0$-plane is coincident with the $x_1 z_1$-plane (fig. 1), thus

$$\left. \begin{array}{l} z_0 = x(\sin \beta \cos \alpha - \cos \beta \cos \delta \sin \alpha) \\[2ex] x_0 = x(\sin \beta \sin \alpha + \cos \beta \cos \delta \cos \alpha) \\[2ex] y_0 = x \cos \beta \sin \delta \end{array} \right\} \qquad (44)$$

Now if z_0 is treated as a function of x_0, y_0, representing the deflected surface in the x_0, y_0, z_0 coordinate system,

$$dz_0 = \frac{\partial z_0}{\partial x_0} dx_0 + \frac{\partial z_0}{\partial y_0} dy_0 \qquad (45)$$

and it can be shown from equations (44) and (45) that:

$$\frac{\partial z_0}{\partial x_0} = \frac{-\sin \delta \cos \alpha \frac{d\beta}{d\theta} + (\sin \beta \cos \delta \cos \alpha - \cos \beta \sin \alpha)\cos \beta \frac{d\delta}{d\theta}}{-\sin \delta \sin \alpha \frac{d\beta}{d\theta} + (\sin \beta \cos \delta \sin \alpha + \cos \beta \cos \alpha)\cos \beta \frac{d\delta}{d\theta}} \tag{46}$$

and

$$\frac{\partial z_0}{\partial y_0} = \frac{\cos \delta \frac{d\beta}{d\theta} + \sin \beta \cos \beta \sin \delta \frac{d\delta}{d\theta}}{-\sin \delta \sin \alpha \frac{d\beta}{d\theta} + (\sin \beta \cos \delta \sin \alpha + \cos \beta \cos \alpha)\cos \beta \frac{d\delta}{d\theta}} \tag{47}$$

Also the square of the length of a line element on the deflected surface is given by

$$ds^2 = dx_0{}^2 + dy_0{}^2 + dz_0{}^2 \tag{48}$$

which upon substitution from equations (44) and (45) yields

$$ds^2 = dx^2 + x^2\left[\left(\frac{d\beta}{d\theta}\right)^2 + \cos^2\beta\left(\frac{d\delta}{d\theta}\right)^2\right]d\theta^2 \tag{49}$$

But inextensibility requires that the metric (eq. (3)) remain unchanged; thus, it follows from equation (49) that:

$$\frac{d\delta}{d\theta} = \pm \frac{1}{\cos \beta}\sqrt{1 - \left(\frac{d\beta}{d\theta}\right)^2} \tag{50}$$

The unit outward normal to the deflected surface is given by

$$\bar{\nu} = \pm \frac{1}{\left[\left(\frac{\partial z_0}{\partial x_0}\right)^2 + \left(\frac{\partial z_0}{\partial y_0}\right)^2 + 1\right]^{1/2}}\left[-\frac{\partial z_0}{\partial x_0}\bar{i} - \frac{\partial z_0}{\partial y_0}\bar{j} + \bar{k}\right] \tag{51}$$

where the positive sign refers to surfaces which are concave downward, and the minus sign to those which are concave upward. The unit normals $\bar{i}$, $\bar{j}$, and $\bar{k}$ are directed along the x_0-, y_0-, and z_0-axes as shown in figure 1. Upon substitution from equations (46), (47), and (50) for $\frac{\partial z_0}{\partial x_0}$, $\frac{\partial z_0}{\partial y_0}$, and $\frac{d\delta}{d\theta}$

equation (51) yields

$$\bar{v} = \left[(\cos \beta \sin \alpha - \sin \beta \cos \delta \cos \alpha) \sqrt{1 - \left(\frac{d\beta}{d\theta}\right)^2} + \sin \delta \cos \alpha \frac{d\beta}{d\theta}\right]\bar{i}$$

$$- \left[\sin \beta \sin \delta \sqrt{1 - \left(\frac{d\beta}{d\theta}\right)^2} + \cos \delta \frac{d\beta}{d\theta}\right]\bar{j}$$

$$+ \left[(\cos \beta \cos \alpha + \sin \beta \cos \delta \sin \alpha) \sqrt{1 - \left(\frac{d\beta}{d\theta}\right)^2} - \sin \delta \sin \alpha \frac{d\beta}{d\theta}\right]\bar{k} \tag{52}$$

The unit tangential vector in the x-direction is given by

$$\bar{\tau}_1 = (\sin \beta \sin \alpha + \cos \beta \cos \delta \cos \alpha)\bar{i}$$

$$+ (\cos \beta \sin \delta)\bar{j} + (\sin \beta \cos \alpha - \cos \beta \cos \delta \sin \alpha)\bar{k} \tag{53}$$

and the unit tangential vector in the θ-direction by

$$\bar{\tau}_2 = \bar{v} \times \bar{\tau}_1$$

$$= \left[-\sin \delta \cos \alpha \sqrt{1 - \left(\frac{d\beta}{d\theta}\right)^2} + (\cos \beta \sin \alpha - \sin \beta \cos \delta \cos \alpha)\frac{d\beta}{d\theta}\right]\bar{i}$$

$$+ \left[\cos \delta \sqrt{1 - \left(\frac{d\beta}{d\theta}\right)^2} - \sin \beta \sin \delta \frac{d\beta}{d\theta}\right]\bar{j}$$

$$+ \left[\sin \delta \sin \alpha \sqrt{1 - \left(\frac{d\beta}{d\theta}\right)^2} + (\cos \beta \cos \alpha + \sin \beta \cos \delta \sin \alpha)\frac{d\beta}{d\theta}\right]\bar{k} \tag{54}$$

The quantity g can be expressed in terms of $\bar{v}$ and $\bar{\tau}_2$ [11] and then in terms of the angle β by using equations (52) and (54):

$$g = x\bar{\tau}_2 \cdot \bar{v},_2 = \frac{-x}{\sqrt{1 - \left(\frac{d\beta}{d\theta}\right)^2}} \left\{\frac{\sin \beta}{\cos \beta}\left[1 - \left(\frac{d\beta}{d\theta}\right)^2\right] + \frac{d^2\beta}{d\theta^2}\right\} \tag{55}$$

Then from equation (6) the function $R(\theta)$ can be expressed in terms of the quantity β as follows:

$$R(\theta) = \frac{-\sqrt{1 - \left(\frac{d\beta}{d\theta}\right)^2}}{\frac{d^2\beta}{d\theta^2} + \frac{\sin\beta}{\cos\beta}\left[1 - \left(\frac{d\beta}{d\theta}\right)^2\right]} \tag{56}$$

APPENDIX B

CALCULATION OF LIFT AND DRAG FORCES ON THE PARAGLIDER WING

In this section the lift and drag forces are derived. As a preliminary
step, the resultant forces applied by the sail to the keel and leading-edge
booms are obtained. These resultant forces and their locations are useful in
obtaining the forces in the shroud lines and spreader bars of the paraglider.

The resultant force applied to the keel by the half of the sail considered
in the analysis is obtained by integration of the stress resultants for the
sail along the keel boundary. Since the tangent vectors along the keel do not
vary with x the vector equation for the force is given by

$$\overline{F}_K = \left(\overline{\tau}_1\right)_K \int_0^{l_K} \left(N_{x\theta}\right)_{\theta=0} dx + \left(\overline{\tau}_2\right)_K \int_0^{l_K} \left(N_\theta\right)_{\theta=0} dx \tag{57}$$

and this force acts through the point $x = x_K$ of the keel, where

$$x_K = \frac{\int_0^{l_K} x\left(N_\theta\right)_{\theta=0} dx}{\int_0^{l_K} \left(N_\theta\right)_{\theta=0} dx} \tag{58}$$

Here $\left(\overline{\tau}_1\right)_K$ and $\left(\overline{\tau}_2\right)_K$ are the unit tangent vectors of the surface at the
keel (eqs. (53) and (54) evaluated at $\theta = 0$). Similarly, the vector equation
for resultant force applied by the sail to the leading-edge boom is given by

$$\overline{F}_L = -\left(\overline{\tau}_1\right)_L \int_0^{l_L} \left(N_{x\theta}\right)_{\theta=\theta_L} dx - \left(\overline{\tau}_2\right)_L \int_0^{l_L} \left(N_\theta\right)_{\theta=\theta_L} dx \tag{59}$$

and this force acts through the point $x = x_L$ of the leading edge where

$$x_L = \frac{\int_0^{l_L} x \left(N_\theta\right)_{\theta=\theta_L} dx}{\int_0^{l_L} \left(N_\theta\right)_{\theta=\theta_L} dx} \tag{60}$$

In equation (59) $\left(\bar{\tau}_1\right)_L$ and $\left(\bar{\tau}_2\right)_L$ are the unit tangent vectors of the surface (eqs. (53) and (54)) at the leading edge $\theta = \theta_L$.

It is necessary now to determine the components of $\bar{F}_K$ and $\bar{F}_L$ in the x_O, y_O, and z_O directions. For example, the component of $\bar{F}_K$ in the x_O direction is given by

$$F_{Kx_O} = \bar{F}_K \cdot \bar{i} = \cos\alpha \int_0^{l_K} \left(N_{x\theta}\right)_{\theta=0} dx + \sin\alpha \left(\frac{d\beta}{d\theta}\right)_{\theta=0} \int_0^{l_K} \left(N_\theta\right)_{\theta=0} dx \tag{61}$$

or for Newtonian impact theory (eq. (39)) in nondimensional form:

$$\frac{F_{Kx_O}}{qS} = -\frac{1}{2}\left(\frac{C}{q l_K^3}\right)\frac{l_K/l_L}{\sin\theta_L}\left[\frac{1}{A}\cos\alpha - \left(\frac{d\beta}{d\theta}\right)_{\theta=0}\sin\alpha\right] \tag{62}$$

Similarly the remaining components are

$$\frac{F_{Ky_O}}{qS} = \frac{1}{2}\left(\frac{C}{q l_K^3}\right)\frac{l_K/l_L}{\sin\theta_L}\sqrt{1 - \left(\frac{d\beta}{d\theta}\right)_{\theta=0}^2} \tag{63}$$

$$\frac{F_{Kz_O}}{qS} = \frac{1}{2}\left(\frac{C}{q l_K^3}\right)\frac{l_K/l_L}{\sin\theta_L}\left[\frac{1}{A}\sin\alpha + \left(\frac{d\beta}{d\theta}\right)_{\theta=0}\cos\alpha\right] \tag{64}$$

$$\frac{F_{Lx_O}}{qS} = \frac{1}{2}\left(\frac{C}{q l_K^3}\right)\frac{(l_K/l_L)^2}{\sin\theta_L}\left(I_1 \frac{\cos\theta_L - l_L/l_K}{\sin\theta_L} - I_2\right) \tag{65}$$

$$\frac{F_{Ly_0}}{qS} = \frac{1}{2}\left(\frac{C}{q{l_K}^3}\right)\frac{(l_K/l_L)^2}{\sin \theta_L}\left(J_1 \ \frac{\cos \theta_L - l_L/l_K}{\sin \theta_L} - J_2\right) \tag{66}$$

$$\frac{F_{Lz_0}}{qS} = \frac{1}{2}\left(\frac{C}{q{l_K}^3}\right)\frac{(l_K/l_L)^2}{\sin \theta_L}\left(K_1 \ \frac{\cos \theta_L - l_L/l_K}{\sin \theta_L} - K_2\right) \tag{67}$$

where

$$I_1 = \sin \beta(\theta_L)\sin \alpha + \cos \beta(\theta_L)\cos \delta(\theta_L)\cos \alpha \tag{68}$$

$$J_1 = \cos \beta(\theta_L)\sin \delta(\theta_L) \tag{69}$$

$$K_1 = \sin \beta(\theta_L)\cos \alpha - \cos \beta(\theta_L)\cos \delta(\theta_L)\sin \alpha \tag{70}$$

$$I_2 = -\sin \delta(\theta_L)\cos \alpha \sqrt{1 - \left(\frac{d\beta}{d\theta}\right)^2_{\theta=\theta_L}}$$
$$+ \left[\cos \beta(\theta_L)\sin \alpha - \sin \beta(\theta_L)\cos \delta(\theta_L)\cos \alpha\right]\left(\frac{d\beta}{d\theta}\right)_{\theta=\theta_L} \tag{71}$$

$$J_2 = \cos \delta(\theta_L)\sqrt{1 - \left(\frac{d\beta}{d\theta}\right)^2_{\theta=\theta_L}} - \sin \beta(\theta_L)\sin \delta(\theta_L)\left(\frac{d\beta}{d\theta}\right)_{\theta=\theta_L} \tag{72}$$

$$K_2 = \sin \delta(\theta_L)\sin \alpha \sqrt{1 - \left(\frac{d\beta}{d\theta}\right)^2_{\theta=\theta_L}}$$
$$+ \left[\cos \beta(\theta_L)\cos \alpha + \sin \beta(\theta_L)\cos \delta(\theta_L)\sin \alpha\right]\left(\frac{d\beta}{d\theta}\right)_{\theta=\theta_L} \tag{73}$$

The coordinates x_{OK}, etc. (fig. 4) through which these forces act may be written with the aid of equations (44), (58), and (60) as

$$x_{OK} = \frac{2}{3} \, l_K \cos \alpha \qquad (74)$$

$$y_{OK} = 0 \qquad (75)$$

$$z_{OK} = -\frac{2}{3} \, l_K \sin \alpha \qquad (76)$$

$$x_{OL} = \frac{2}{3} \, l_L I_1 \qquad (77)$$

$$y_{OL} = \frac{2}{3} \, l_L J_1 \qquad (78)$$

$$z_{OL} = \frac{2}{3} \, l_L K_1 \qquad (79)$$

Finally, when both halves of the symmetrical sail are considered (fig. 4), the lift and drag coefficients can be expressed as follows:

$$C_L = \frac{L}{qS}$$

$$= \frac{2}{qS}\left(F_{Kz_0} + F_{Lz_0}\right) \qquad (80)$$

$$C_D = \frac{D}{qS}$$

$$= \frac{2}{qS}\left(F_{Kx_0} + F_{Lx_0}\right) \qquad (81)$$

where L and D are the lift and drag forces, respectively, on the wing; $q = \frac{1}{2}\rho V^2$ is the dynamic pressure, and

$$S = l_K l_L \sin \theta_L \qquad (82)$$

is the total surface area of the sail. The resultant of the lift and drag forces acts through the point $\left(\bar{x}_0, \bar{y}_0\right)$ where

$$\bar{x}_0 = \frac{x_{OL}F_{Lz_0} + x_{OK}F_{Kz_0}}{F_{Lz_0} + F_{Kz_0}} \tag{83}$$

and

$$\bar{z}_0 = \frac{z_{OL}F_{Lx_0} + z_{OK}F_{Kx_0}}{F_{Lx_0} + F_{Kx_0}} \tag{84}$$

Equations (80) and (81) have been used to obtain the results shown in figures 7 and 8.

REFERENCES

1. Rogallo, Francis M., Lowry, John G., Croom, Delwin R., and Taylor, Robert T.: Preliminary Investigation of a Paraglider. NASA TN D-443, 1960.

2. Naeseth, Rodger L.: An Exploratory Study of a Parawing as a High-Lift Device for Aircraft. NASA TN D-629, 1960.

3. Hewes, Donald E.: Free-Flight Investigation of Radio-Controlled Models With Parawings. NASA TN D-927, 1961.

4. Taylor, Robert T.: Wind-Tunnel Investigation of Paraglider Models at Supersonic Speeds. NASA TN D-985, 1961.

5. Fournier, Paul G., and Bell, B. Ann: Low Subsonic Pressure Distributions on Three Rigid Wings Simulating Paragliders With Varied Canopy Curvatures and Leading-Edge Sweep. NASA TN D-983, 1961.

6. Fournier, Paul G., and Bell, B. Ann: Transonic Pressure Distributions on Three Rigid Wings Simulating Paragliders With Varied Canopy Curvature and Leading-Edge Sweep. NASA TN D-1009, 1962.

7. Penland, Jim A.: A Study of the Aerodynamic Characteristics of a Fixed Geometry Paraglider Configuration and Three Canopies With Simulated Variable Canopy Inflation at a Mach Number of 6.6. NASA TN D-1022, 1962.

8. Johnson, Joseph L., Jr., and Hassell, James L., Jr.: Summary of Results Obtained in Full-Scale Tunnel Investigation of the Ryan Flex-Wing Airplane. NASA TM SX-727, 1962.

9. Truitt, Robert Wesley: Hypersonic Aerodynamics. The Roland Press, New York, 1959.

10. Hayes, W. D., and Probstein, R. F.: Hypersonic Flow Theory. Academic Press, New York, 1959.

11. Struik, D. J.: Lectures on Classical Differential Geometry, Addison-Wesley
    Press, Cambridge, Mass., 1950, ch. 2.

12. Goldenveizer, A. L.: Theory of Elastic Thin Shells, Pergamon Press,
    New York, 1961. Translation from Russian edition, 1953, ch. 6.

TABLE 1.- FORCE CHARACTERISTICS OF A PARAGLIDER WING

AT VARIOUS ANGLES OF ATTACK, α

$$\left[\frac{l_K}{l_L} = 1;\ \theta_L = 45°;\ \beta\left(\theta_L\right) = 0;\ \delta\left(\theta_L\right) = 28.2°;\ \frac{d}{l_K} = 0.4872\right]$$

α, deg	25	30	35	40	45	50	55
$(d\beta/d\theta)_0$	0.99895	0.99603	0.99234	0.98834	0.98433	0.9804	0.9767
c/ql_K^3	.004135	.01046	.01979	.03218	.04716	.06450	.08343
F_{Kx_0}/qS	.000137	.00103	.00322	.00724	.0134	.0221	.0332
F_{Ky_0}/qS	.000134	.000658	.00173	.00346	.00588	.00899	.0127
F_{Kz_0}/qS	.00316	.00791	.0147	.0233	.0330	.0432	.0531
F_{Lx_0}/qS	.000791	.00244	.00548	.0103	.0173	.0265	.0379
F_{Ly_0}/qS	-.00244	-.00578	-.0103	-.0159	-.0221	-.0289	-.0357
F_{Lz_0}/qS	.00185	.00497	.00967	.0157	.0227	.0300	.0369
x_{OK}/l_K	.604	.577	.546	.511	.471	.428	.382
y_{OK}/l_K	0	0	0	0	0	0	0
z_{OK}/l_K	-.282	-.333	-.382	-.428	-.471	-.511	-.546
x_{OL}/l_K	.533	.508	.481	.450	.415	.377	.336
y_{OL}/l_K	.315	.315	.315	.315	.315	.315	.315
z_{OL}/l_K	-.248	-.294	-.337	-.377	-.416	-.450	-.482
C_L	.0100	.0258	.0487	.0780	.111	.146	.180
C_D	.00185	.00695	.0174	.0351	.0615	.0973	.142
L/D	5.40	3.71	2.80	2.22	1.81	1.51	1.27
$\bar{x}_0/l_K$	.578	.551	.520	.486	.449	.408	.364
$\bar{z}_0/l_K$	-.253	-.306	-.354	-.398	-.440	-.478	-.512

TABLE 1.- FORCE CHARACTERISTICS OF A PARAGLIDER WING

AT VARIOUS ANGLES OF ATTACK, α - Concluded

α, deg	60	65	70	75	80	85	90
$(d\beta/d\theta)_0$	0.9732	0.9698	0.9665	0.9639	0.9597	0.9562	0.9527
$C/q l_K^3$	.1035	.1243	.1445	.1648	.1832	.2003	.2145
F_{Kx_0}/qS	.0465	.0619	.0783	.0959	.113	.130	.144
F_{Ky_0}/qS	.0168	.0214	.0262	.0314	.0364	.0415	.0461
F_{Kz_0}/qS	.0619	.0690	.0735	.0757	.0744	.0702	.0628
F_{Lx_0}/qS	.0512	.0662	.0822	.0991	.115	.131	.144
F_{Ly_0}/qS	-.0426	-.0492	-.0550	-.0604	-.0648	-.0683	-.0703
F_{Lz_0}/qS	.0429	.0473	.0496	.0495	.0468	.0415	.0336
x_{OK}/l_K	.333	.282	.228	.172	.116	.0581	0
y_{OK}/l_K	0	0	0	0	0	0	0
z_{OK}/l_K	-.577	-.604	-.626	-.644	-.656	-.664	-.667
x_{OL}/l_K	.293	.248	.200	.151	.102	.0514	0
y_{OL}/l_K	.315	.315	.315	.315	.315	.315	.315
z_{OL}/l_K	-.509	-.532	-.552	-.568	-.579	-.585	-.587
C_L	.209	.233	.246	.250	.242	.223	.193
C_D	.195	.256	.321	.390	.457	.521	.578
L/D	1.07	.908	.767	.642	.531	.429	.334
$\bar{x}_0/l_K$	.317	.268	.217	.164	.110	.0556	0
$\bar{z}_0/l_L$	-.542	-.567	-.589	-.605	-.617	-.624	-.627

TABLE 2.- FORCE CHARACTERISTICS OF A PARAGLIDER WING

AT VARIOUS DIHEDRAL ANGLES, $\beta(\theta_L)$

$$\left[\frac{l_K}{l_L} = 1; \ \theta_L = 45^\circ; \ \frac{d}{l_K} = 0.4872; \ \alpha = 35^\circ\right]$$

| $\beta(\theta_L)$, deg	-15	-10	-5	0	5	10	14.4
$(d\beta/d\theta)_0$	0.98727	0.98702	0.98905	0.99234	0.99574	0.99842	0.99970
$c/q l_K^3$	.01894	.02126	.02153	.01979	.01645	.01190	.007500
F_{Kx_0}/qS	.00304	.00341	.00347	.00322	.00270	.00196	.00124
F_{Ky_0}/qS	.00213	.00241	.00225	.00173	.00107	.000473	.000130
F_{Kz_0}/qS	.0140	.0157	.0160	.0147	.0123	.00888	.00560
F_{Lx_0}/qS	.00778	.00787	.00701	.00548	.00366	.00192	.000760
F_{Ly_0}/qS	-.00633	-.00859	-.0100	-.0103	-.00935	-.00723	-.00475
F_{Lz_0}/qS	.0105	.0114	.0110	.00967	.00760	.00520	.00313
x_{OK}/l_K	.546	.546	.546	.546	.546	.546	.546
y_{OK}/l_K	0	0	0	0	0	0	0
z_{OK}/l_K	-.382	-.382	-.382	-.382	-.382	-.382	-.382
x_{OL}/l_K	.383	.415	.448	.481	.515	.548	.576
y_{OL}/l_K	.264	.293	.310	.315	.310	.293	.368
z_{OL}/l_K	-.478	-.431	-.384	-.337	-.289	-.242	-.201
C_L	.0490	.0542	.0540	.0487	.0397	.0281	.0175
C_D	.0216	.0226	.0210	.0174	.0127	.00777	.00400
L/D	2.26	2.40	2.57	2.80	3.12	3.62	4.37
$\bar{x}_0/l_K$	.476	.491	.506	.520	.534	.547	.557
$\bar{z}_0/l_K$	-.451	-.417	-.384	-.354	-.329	-.313	-.314
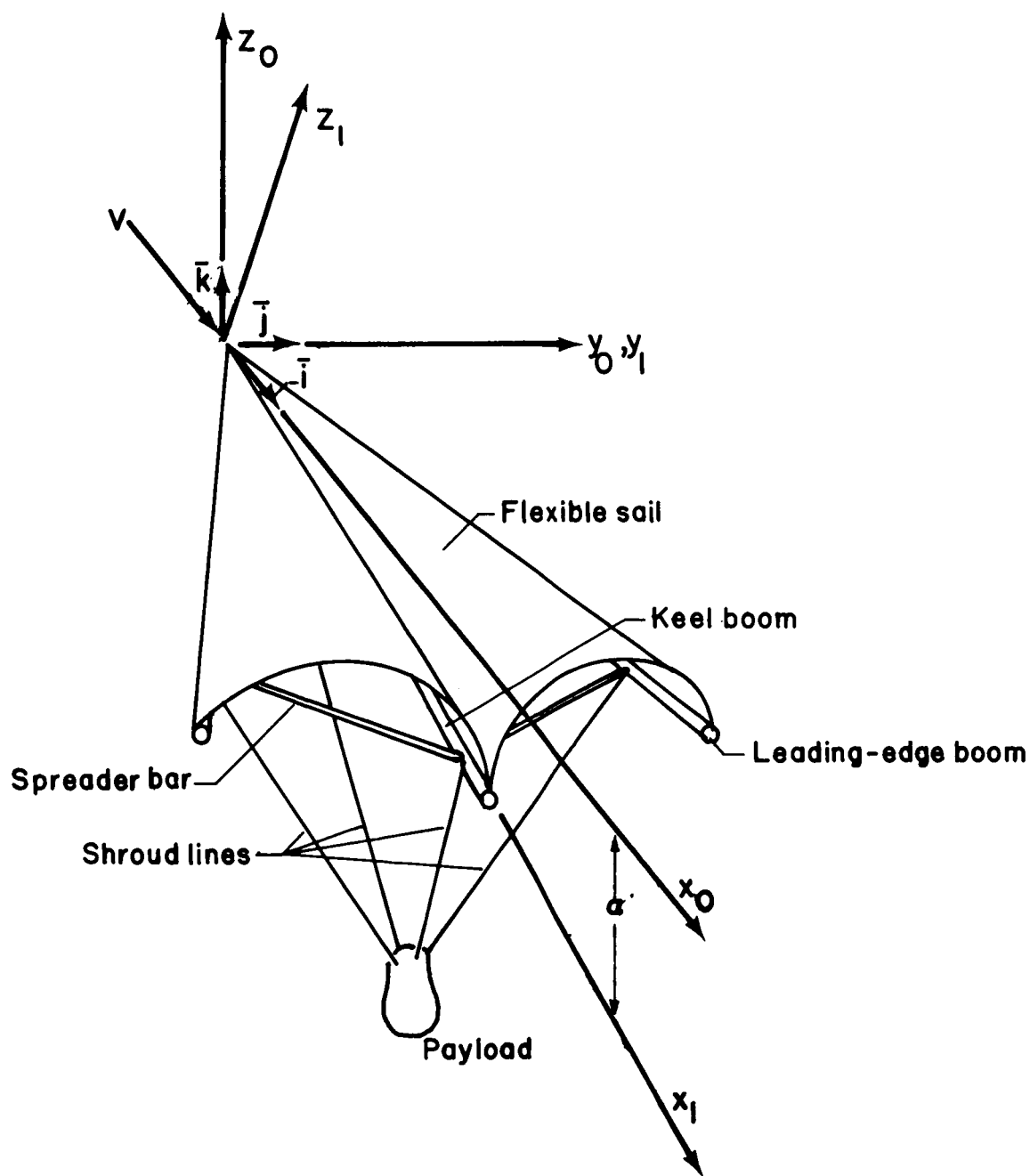
NASA

Figure 1.- Paraglider wing configuration.
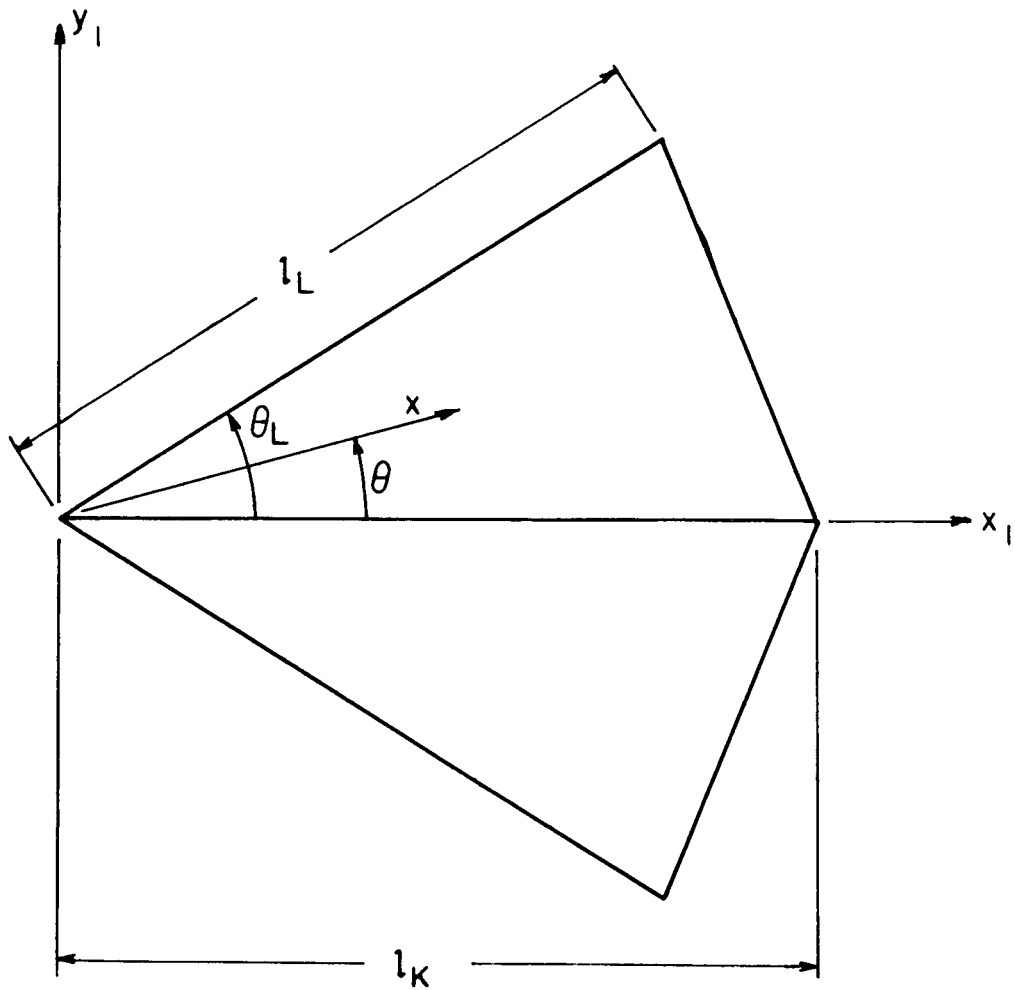
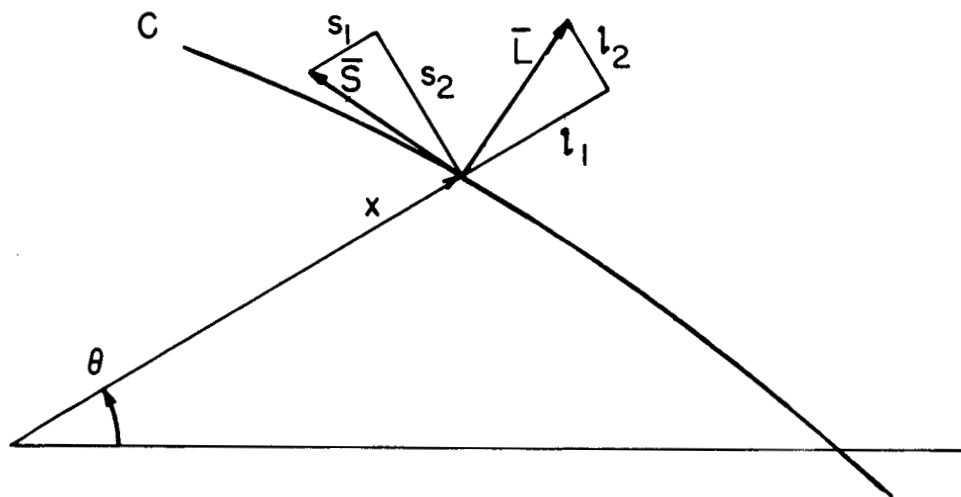(a) Unloaded surface of sail.   NASA

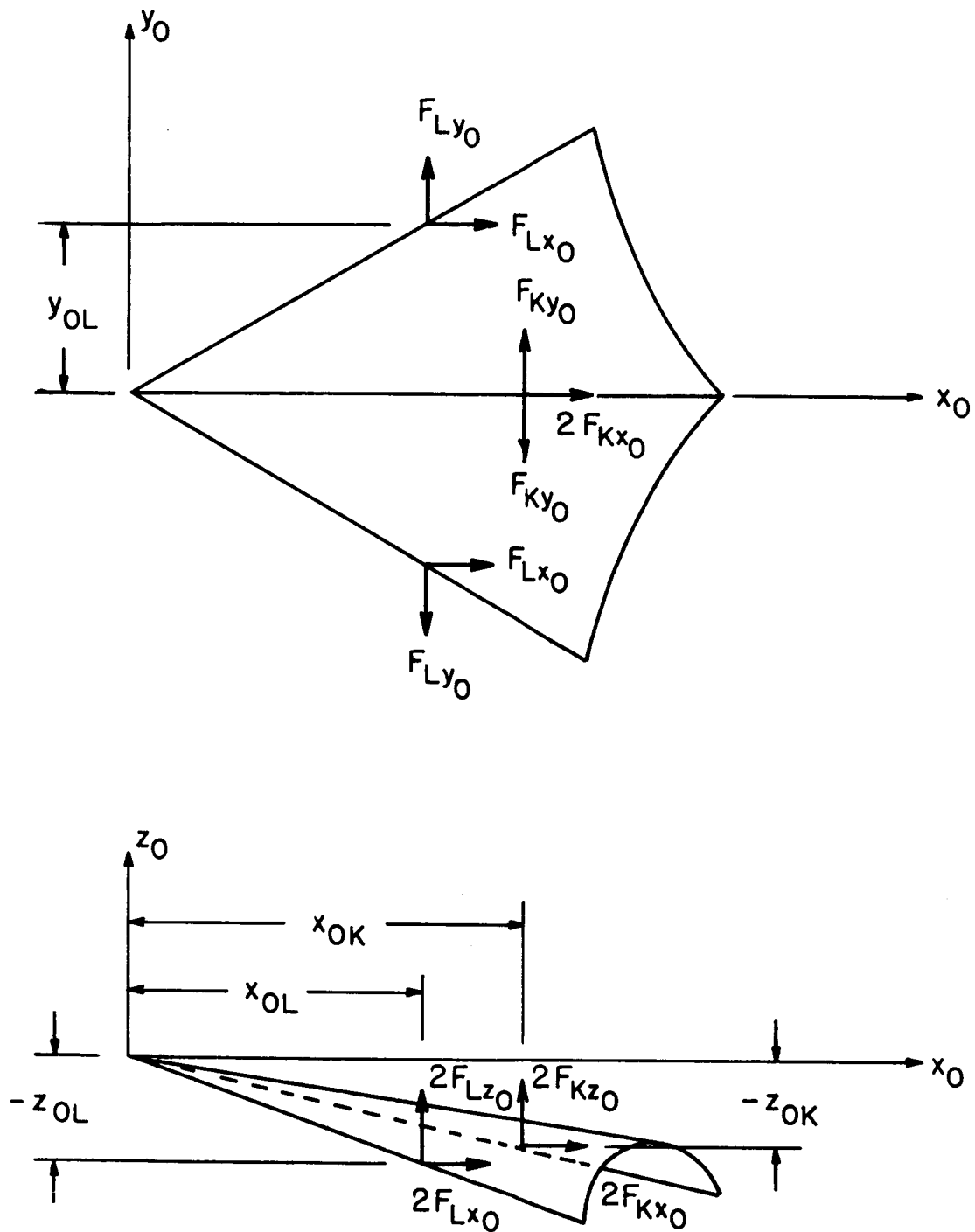Figure 2.- Coordinates of sail.
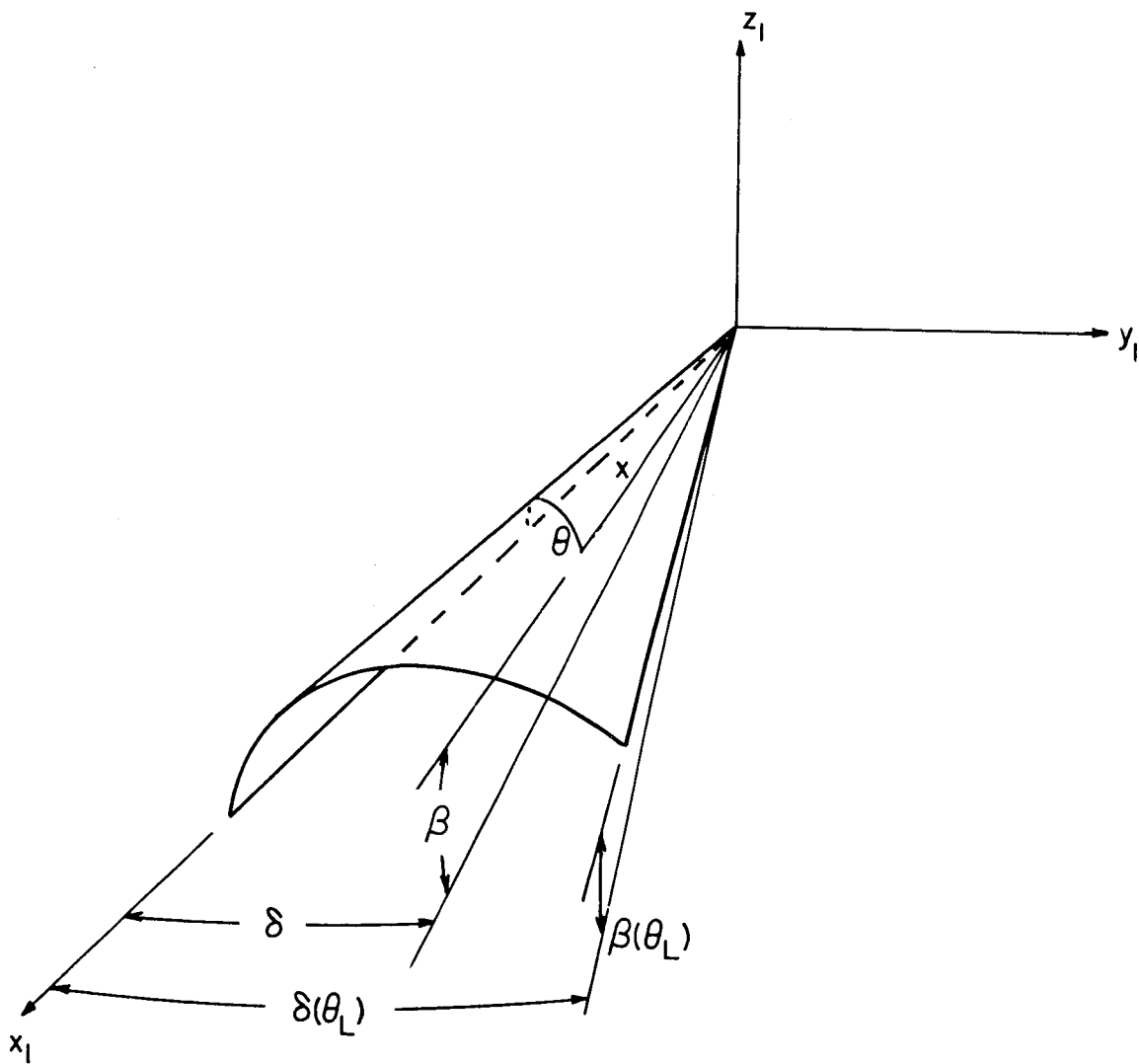
(b) Loaded surface of sail.   NASA

Figure 2.- Concluded.

Figure 3.- Boundary vectors.

NASA

Figure 4.- Resultant forces applied by the sail to the keel and
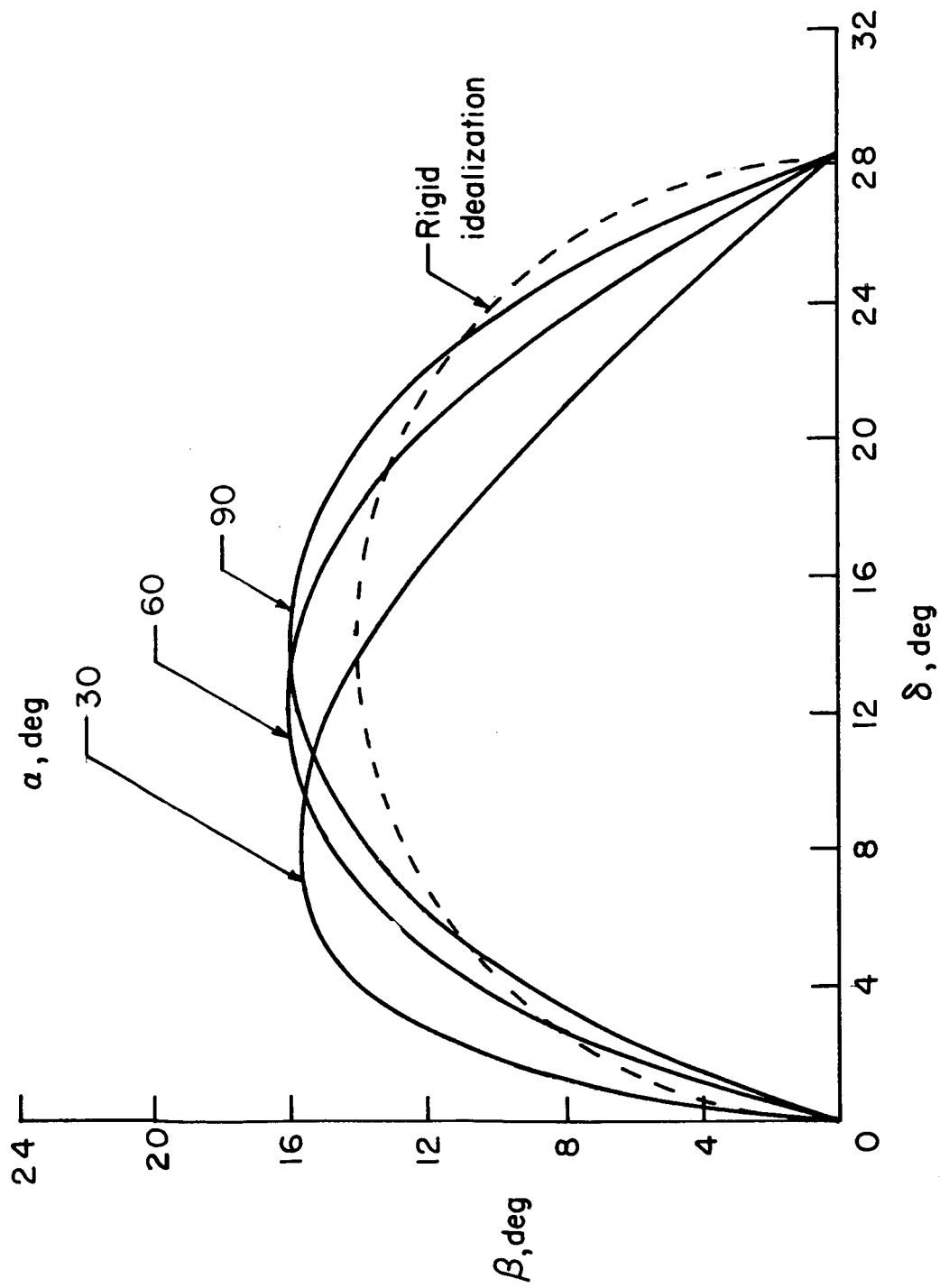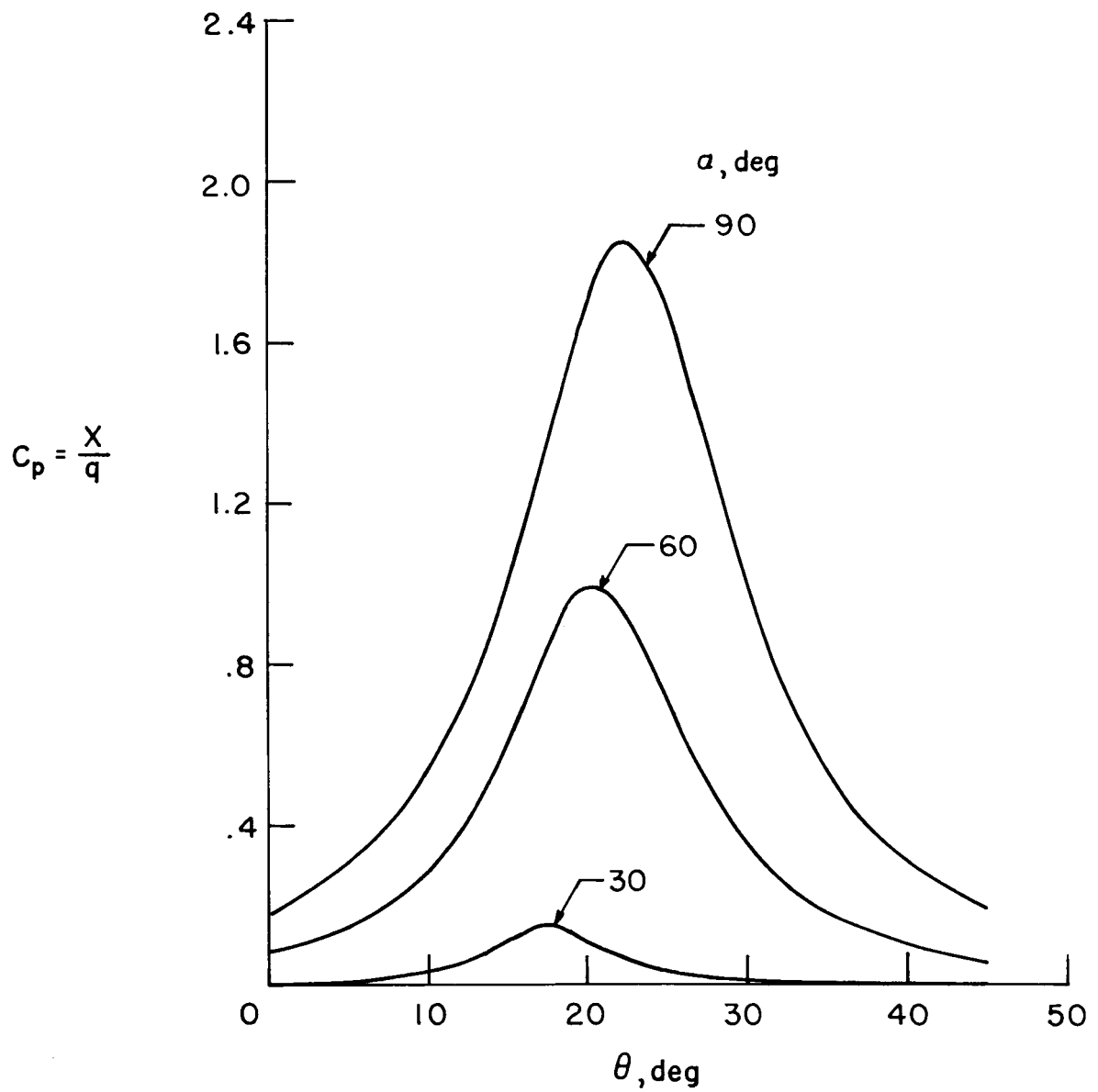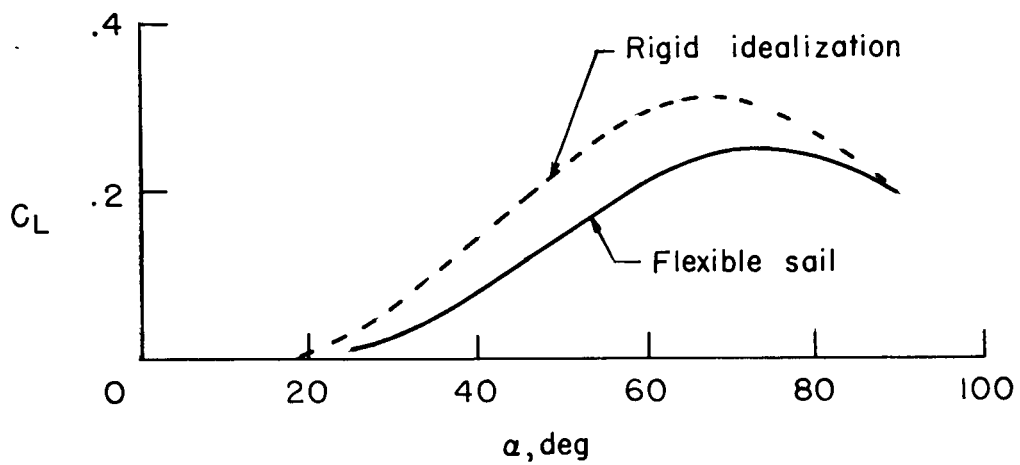leading-edge booms.

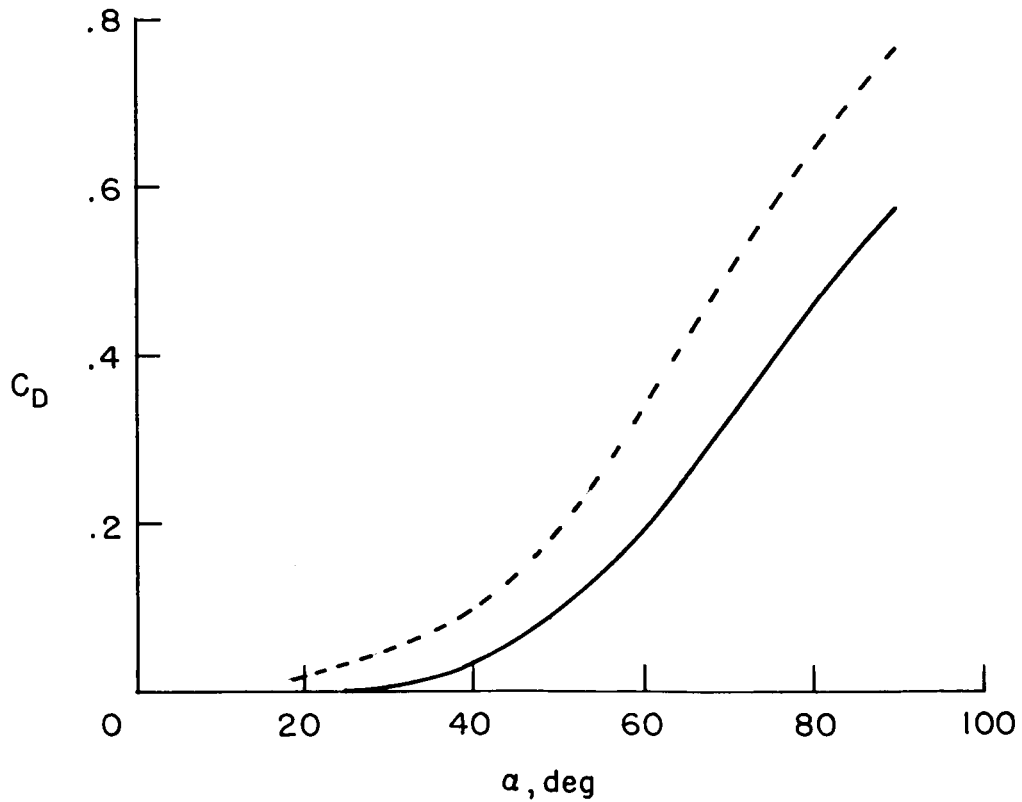Figure 5.- Variation of deflected shape of surface with angle of attack.

NASA

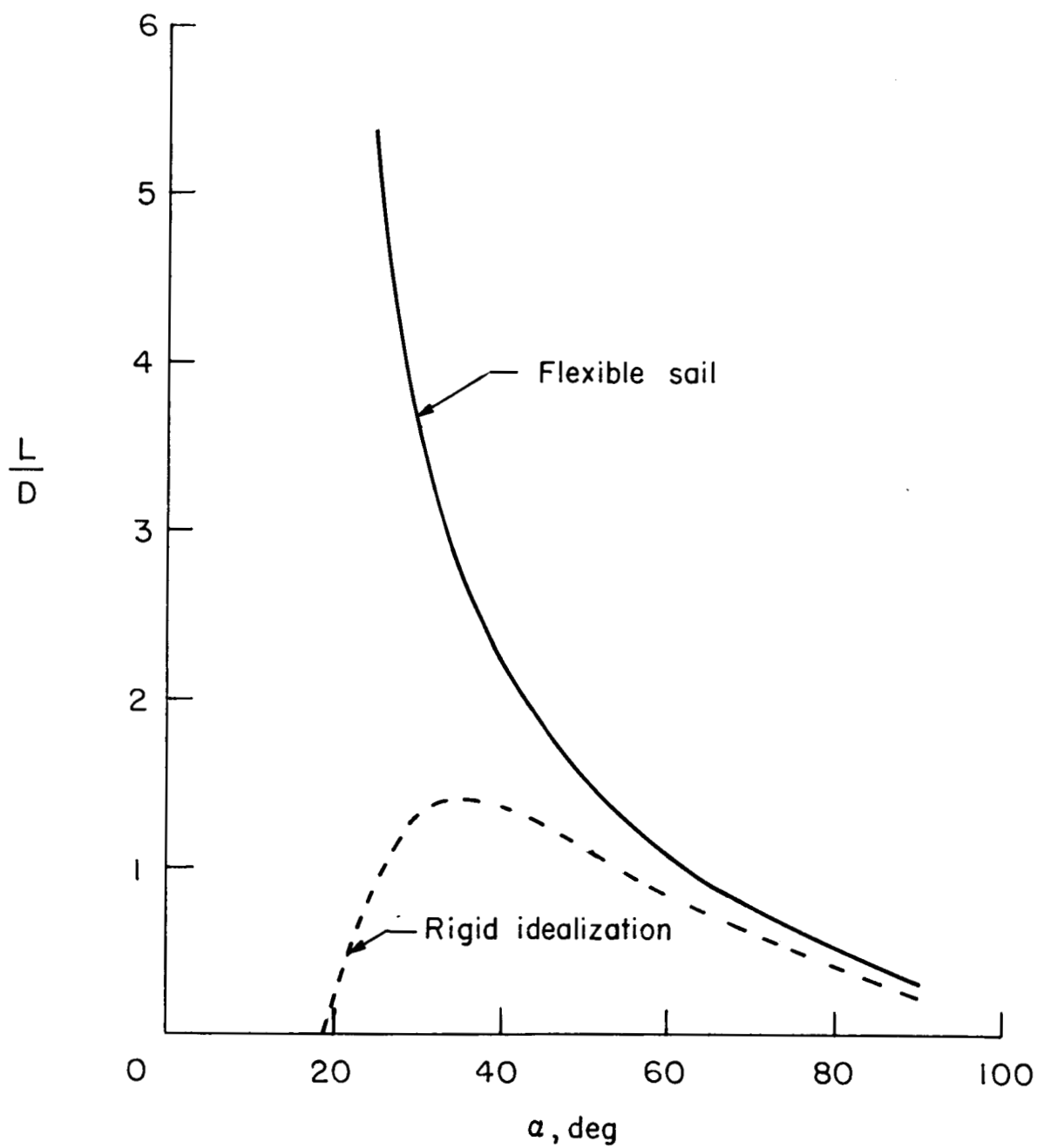Figure 6.- Variation of pressure coefficient with angle of attack.

(a) Lift.

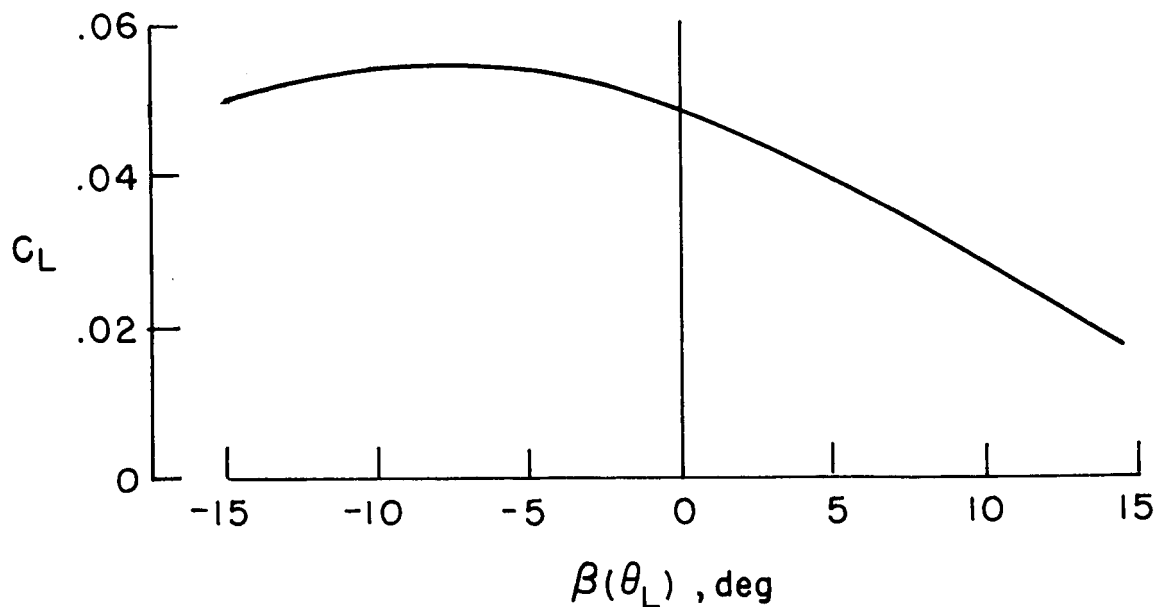(b) Drag.   NASA

Figure 7.- Comparison of lift and drag characteristics of paraglider wing with those of the rigid idealization.
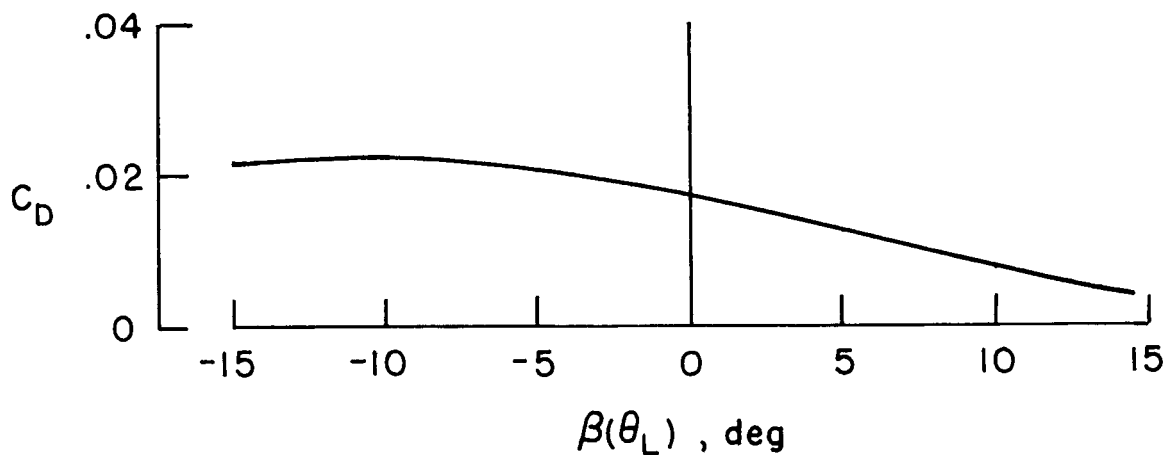
(c) Lift-to-drag ratio.   NASA

Figure 7.- Concluded.

(a) Lift.

(b) Drag.   NASA

Figure 8.- Variation of lift and drag characteristics of paraglider
   wing with dihedral angle $\beta(\theta_L)$. Angle of attack, $\alpha = 35^\circ$.